

# Spin polarized tunneling in ferromagnet/unconventional superconductor junctions

Igor Žutić and Oriol T. Valls

Department of Physics and Minnesota Supercomputer Institute, University of Minnesota, Minneapolis, Minnesota 55455  
(November 16, 1998)

We study tunneling in ferromagnet/unconventional superconductor (F/S) junctions. We include the effects of spin polarization, interfacial resistance, and Fermi wavevector mismatch (FWM) between the F and S regions. Andreev reflection (AR) at the F/S interface, governing tunneling at low bias voltage, is strongly modified by these parameters. The conductance exhibits a wide variety of novel features as a function of applied voltage.

74.80.Fp, 74.50+r, 74.72-h

Spin polarized transport and tunneling between ferromagnetic and superconducting materials has become a vigorously pursued area of research. The studies performed [1–5] have implications for the understanding of unconventional superconductivity and for the development of devices using spin polarized current [1,2,6]. A recent study of a ferromagnet/unconventional superconductor (F/S) system has revealed [5] a differential conductance dip at zero bias (ZBCD), attributed to suppression of Andreev reflection (AR) as a consequence of high spin polarization in the ferromagnet. While there is substantial work [1,2,7,8] on the interplay of ferromagnetism and superconductivity in tunneling properties involving *s*-wave superconductors, there is still no adequate theory for these phenomena in the context of unconventional superconductivity. Replacing an *s*-wave superconductor by an unconventional one in a normal metal/superconductor (N/S) structure can drastically alter the conductance spectrum [9–11], and important changes should also occur when such replacement is made in a F/S structure. For N/S junctions, zero bias conductance peaks (ZBCP) observed in HTSC's are interpreted as arising from the sign change of the pair potential (PP) which leads to the formation [9] of midgap surface states. The spectral weight of these states has, for a  $d_{x^2-y^2}$  state, a maximum for (110) oriented surfaces and vanishes for (100) surfaces. The absence of ZBCP in  $\text{Nd}_{1.85}\text{Ce}_{0.15}\text{CuO}_4$  is considered evidence [10] for a dominant *s*-wave component.

Previously published work on tunneling in unconventional superconductors examined the unpolarized case [9,11], or [1,2,8] F/S junctions with an *s*-wave PP [12]. Here we consider the theory of tunneling spectroscopy for an F/S junction with arbitrary spin polarization. We investigate the interplay of ferromagnetism and unconventional superconductivity in forming ZBCP, ZBCD, and other features at finite bias. We include the effects of the exchange energy (related to the degree of polarization) interfacial barrier height and Fermi wavevector mismatch (FWM) in the magnitude of the Fermi wavevectors in the F and S regions. Variation of these parameters leads to rich behavior and novel features in the conductance, which require careful interpretation. Thus, FWM

and spin polarization can combine to yield a ZBCP in an *s*-wave superconductor, while if one neglects FWM [1,2,8,12] the effect of spin polarization invariably leads to suppression of AR.

We solve the Bogoliubov-de Gennes (BdG) equations [8,9,11,13] for a ballistic F/S junction. We extend the usual one-body Hamiltonian approach of Ref. [8] to include: 1) scattering at the F/S interface,  $x = 0$ , modeled by a potential  $V(\mathbf{r}) = H\delta(x)$ , where  $H$  is the strength of the potential barrier, and 2) allow for FWM, i.e.  $E_F = \hbar^2 k_F^2 / 2m$  in the F region at  $x < 0$  (  $E_F$  is the spin averaged value,  $E_F = (\hbar^2 k_{F\uparrow}^2 / 2m + \hbar^2 k_{F\downarrow}^2 / 2m) / 2$ ), and  $E'_F = \hbar^2 k_F'^2 / 2m$  in the S region at  $x > 0$ . We include the exchange energy [8]  $h(\mathbf{r}) = h_0\Theta(-x)$ , ( $\Theta(x)$  is a step function) and the pair potential [9,11]  $\Delta(\mathbf{k}', \mathbf{r}) = \Delta(\mathbf{k}', \mathbf{r})\Theta(x)$ . From the invariance of the Hamiltonian with respect to translations parallel to  $x = 0$ , the parallel component of the wave vector is conserved at the junction [11,13]. Then, the parallel component of the solutions of the BdG equations is a plane wave, and the problem reduces to a 1D one.

For an electron injected from the F side, with spin  $S = \uparrow, \downarrow$ , excitation energy  $\epsilon$ , and wavevector  $\mathbf{k}_S^+$  at an angle  $\theta$  from the interface normal, there are (without spin-flip scattering) four scattering processes [11,14] with different amplitudes. For specular reflection at the interface, these are: 1) Andreev reflection [8,13,15] with amplitude  $a_S$  as a hole with spin, wavevector, and angle with the interface normal,  $\bar{S}$  (opposite to  $S$ ),  $\mathbf{k}_{\bar{S}}^-$ , and  $\theta_{\bar{S}}$ , respectively. 2) Ordinary reflection with amplitude  $b_S$  as an electron with variables  $S$ ,  $-\mathbf{k}_S^+$ ,  $-\theta$ . 3) Transmission with amplitude  $c_S$  as an electronlike quasiparticle (ELQ) with  $\mathbf{k}_S'^+$  and  $\theta_S'$ . 4) Transmission (amplitude  $d_S$ ) as a holelike quasiparticle (HLQ) defined by  $-\mathbf{k}_S'^-$ , and  $-\theta_S'$ . Here we have used [8,11]  $k_S^{\pm} \approx k_{FS}$  and  $k_S'^{\pm} \approx k_F'$ , as explained below. The ELQ and HLQ have different, spin dependent, wavevectors, and therefore they feel different pair potentials  $\Delta_{S+}$  and  $\Delta_{S-}$ , with  $\Delta_{S\pm} = |\Delta_{S\pm}| \exp(i\phi_{S\pm})$ . The spin dependence (even without FWM) of wavevectors and PP's is a novel feature of F/S junctions.

Conservation of  $k_{\parallel S}$  yields the analogue of Snell's law,  $k_{FS} \sin \theta = k_F' \sin \theta_S'$ ,  $S = \uparrow, \downarrow$ , and for  $k_{FS} > k_F'$

there is a spin dependent angle of total reflection. For a PP of the  $d_{x^2-y^2}$  form, and allowing for different angles  $\alpha \in (-\pi/2, \pi/2)$  between the crystallographic  $a$ -axis and the interface normal, we have  $\Delta_{S\pm} = \Delta_0 \cos(2\theta'_{S\pm})$ , where  $\theta'_{S\pm}$  are related to  $\theta'_S$  (and thus to the incident angle  $\theta$ , from ‘‘Snell’s law’’) by  $\theta'_{S\pm} = \theta'_S \mp \alpha$ . The spin dependence of these angles will produce more complicated conductance features.

In solving the BdG equations in the direction normal to the interface, we have for the magnitude of the relevant wavevectors: in the F region,  $k_S^\pm = (2m/\hbar^2)^{1/2}[E_F \pm \epsilon + \rho_S h_0]^{1/2}$ , where  $\rho_S = \pm 1$  for  $S = \uparrow (\downarrow)$ , and in the S region,  $k'_S^\pm = (2m/\hbar^2)^{1/2}[E'_F \pm (\epsilon^2 - |\Delta_{S\pm}|^2)^{1/2}]^{1/2}$ . In the regime of interest,  $E_F, E'_F \gg \max(\epsilon, |\Delta_{S\pm}|)$  and [8,11,16] we have  $k_S^\pm \approx k_{FS} \equiv (2m/\hbar^2)^{1/2}[E_F + \rho_S h_0]^{1/2}$ ,  $k'_S^\pm \approx k'_F$ . From this and ‘‘Snell’s law’’, the components of  $\mathbf{k}_S^\pm$  and  $\mathbf{k}'_S^\pm$  normal and parallel to the interface can be found. We write  $\mathbf{k}_S^\pm \equiv (k_S, k_{\parallel S})$ , and  $\mathbf{k}'_S^\pm \equiv (k'_S, k_{\parallel S})$ , in the F and S regions.

The conductance spectrum is calculated via the Blonder-Tinkham-Klapwijk (BTK) method [14] extended to include unconventional superconductivity [11] and net spin polarization. It is sufficient [11,14] to calculate  $a_S$  and  $b_S$ :

$$a_S = \frac{4t_S L_S \Gamma_+ e^{-i\phi_{S+}}}{U_{SS+} U_{\bar{S}S-} - V_{SS-} V_{\bar{S}S+} \Gamma_+ \Gamma_- e^{i(\phi_{S-} - \phi_{S+})}} \quad (1)$$

$$b_S = \frac{V_{SS+} U_{\bar{S}S-} - U_{SS-} V_{\bar{S}S+} \Gamma_+ \Gamma_- e^{i(\phi_{S-} - \phi_{S+})}}{U_{SS+} U_{\bar{S}S-} - V_{SS-} V_{\bar{S}S+} \Gamma_+ \Gamma_- e^{i(\phi_{S-} - \phi_{S+})}} \quad (2)$$

where we introduce  $\Gamma_\pm \equiv (\epsilon - (\epsilon^2 - |\Delta_{S\pm}|^2)^{1/2})/|\Delta_{S\pm}|$ ,  $L_S \equiv L_0 \cos \theta'_S / \cos \theta$ ,  $L_0 \equiv k'_F/k_F$ , describing FWM,  $t_S \equiv (1 + \rho_S X)^{1/2}$ ,  $t_{\bar{S}} \equiv (1 - \rho_S X)^{1/2} \cos \theta_{\bar{S}} / \cos \theta$ ,  $X \equiv h_0/E_F$ , which defines the degree of polarization,  $U_{\bar{S}S\pm} \equiv t_{\bar{S}} + w_{S\pm}$ ,  $V_{SS\pm} \equiv t_S - w_{S\pm}$ ,  $w_{S\pm} \equiv L_S \pm 2iZ$ ,  $Z \equiv Z_0/\cos \theta$ , and  $Z_0 \equiv mH/\hbar k_F$  is the interfacial barrier parameter. The normalized differential conductance [11] (in units of  $e^2/h$ ) is then

$$G \equiv G_\uparrow + G_\downarrow = \sum_{S=\uparrow, \downarrow} P_S \left( 1 + \frac{k_{\bar{S}}}{k_S} |a_S|^2 - |b_S|^2 \right) \quad (3)$$

where the probabilities of an incident electron with spin  $S$ ,  $P_S$ , satisfy [8],  $P_\uparrow/P_\downarrow = (1+X)/(1-X)$ . At  $X = 0$  we recover the results of Ref. [11]. The ratio of wavevectors in Eq. (3) reflects that the incident electron and the AR hole belong to different spin bands. One can use the conservation of probability current [14] to generalize the sum rule for the reflection coefficients in the case of subgap conductance ( $E < |\Delta_{S\pm}|$ ), for the unpolarized case. We get  $\frac{k_{\bar{S}}}{k_S} |a_S|^2 + |b_S|^2 = 1$  and then  $G_S$  can be expressed in terms of the AR amplitude only. For  $k_{FS} > k'_F$ , one sees from Eq. (3) and ‘‘Snell’s law’’, that for  $|\theta|$  greater than the angle of total reflection ( $a_S = 0$ )  $G_S = 0$ . We define

the angularly averaged (AA) conductance [11],  $\langle G_S \rangle$ , as  $\langle G_S \rangle = \int_{\Omega_S} d\theta \cos \theta G(\theta) / \int_{\Omega_S} d\theta \cos \theta$ , where  $\Omega_S$  is limited by the angle of total reflection or by experimental setup.

We concentrate on the  $d_{x^2-y^2}$  state and take parameter values appropriate for HTSC’s and ongoing experiments [17] on the effect of spin polarization on  $G$ . Typically there is a small interface resistance [5] i.e. small  $Z_0$  values, away from the tunneling limit  $Z_0 \gg 1$  [7]. The experiments use [5] half-metallic ferromagnets with  $X \rightarrow 1$  and FWM values of  $L_0 < 1$  [17]. We present our results for  $G$  and  $\langle G \rangle$  as a function of dimensionless energy  $E \equiv eV/\Delta_0$ , where  $V$  is the bias voltage. We take  $E'_F/\Delta_0 = 12.5$ , with  $E_F = E'_F$  ( $L_0 = 1$ ) and  $E_F = 4E'_F$  ( $L_0 = 1/2$ ), to consider the influence of FWM.

In Fig. 1, we show results for  $G(E)$  at  $\theta = 0$ , and  $\alpha = 0$  (i.e. an F/S interface along the (100) plane). This behavior is the same as for an  $s$ -wave superconductor ( $\Delta_{S\pm} = \Delta_0$ ). In panel (a), at zero interfacial barrier, we display the effect of increasing  $X$ . The solid lines represent results with FWM,  $L_0 = 1/2$ . The behavior of the amplitude of  $G$  at zero bias (AZB) reflects the interplay between the effects of FWM and ferromagnetism. At  $X = 0$  there is a ZBCD, as in previous work [18]. This is caused by the effective barrier introduced by FWM (even at  $Z_0 = 0$ ), at the interface which separates regions with different Fermi energies. With increased exchange energy the ZBCD evolves into a ZBCP, which narrows with decreasing  $L_0$ . The ZBCP in this case is not due to unconventional superconductivity, since there is no sign change in the PP’s experienced by ELQ and HLQ. For reasonable values of the FWM, the maximum AZB is 2, independent of  $X$ . The AZB maximum is obtained from the condition  $k_\uparrow k_\downarrow = k_S'^2 \equiv k_F'^2$ . For  $L_0 = 1/2$ , this occurs at  $X \approx 0.968$ . Thus, in the presence of FWM Andreev reflection can be enhanced by spin polarization and can even become maximal at a special value of  $X$ . These results differ from those obtained without FWM when AR is always suppressed and  $G$  decreases with  $X$ . The dashed lines (no FWM) illustrate this point. In panel (b) we show the influence of barrier strength at fixed  $X = 0.6$ . In the presence of FWM the subgap conductance is more reduced, with sharper peaks at  $E = 1$  than for the same  $Z_0$  at  $L_0 = 1$  (dashed lines), since the effective barrier strength [18] is enhanced.

In Fig. 2 we use the same parameter values and notation as in Fig. 1 to display the effect of AA on  $G$  for  $s$ -wave ( $\Delta_{S\pm} = \Delta_0$  for all angles). In panel (a) the solid curves, (with FWM) show that the ZBCP at fixed  $X$  remains after AA, while its amplitude is typically reduced. We see that, unlike in the unpolarized case [18], FWM can actually enhance  $G(0)$  at fixed polarization. In panel (b) we show that the effects of interfacial barrier on  $\langle G \rangle$  are similar to those given in Fig. 1.

We now turn to the effects of the sign change of the PP, i.e., of the unconventional nature of the S region. We take

$\alpha \neq 0$  and  $\theta \neq 0$  so that ELQ and HLQ may feel PP's of opposite sign. First, in Fig. 3, we consider the limit of no FWM, with  $\theta = \pi/12$  and  $\alpha = \pi/4$ . We examine the dependence of the AZB on  $X$  and  $Z_0$ . In panel (a) we see that the ZBCD becomes more pronounced with higher  $X$ , because of suppressed AR. In the limit  $(E_F - h_0) \rightarrow 0$ , the subgap conductance vanishes, due to the vanishing of the minority spin density of states (see the bottom-most curve). For  $X = 0.4$  there appears a finite bias peak (FBCP), which moves to lower energy with increasing  $X$ . This follows from "Snell's law". At larger  $X$ , there will be increased difference between  $k_S$  and  $k'_S$ , and  $\theta'_S$  will depart more from  $\theta$ . ELQ and HLQ feel PP's with increasingly different spin dependent magnitude:  $G_\uparrow$  and  $G_\downarrow$  are governed by different energy scales. When  $\alpha \neq 0, \pi/4$ ,  $G(E)$  displays two or four distinct features determined by up to four different PP values. In panel (b) we show the decomposition of the  $X = 0.6$  result into its  $G_\uparrow$  and  $G_\downarrow$  components. The position of the FBCP, discussed above, is at the maximum of  $G_\downarrow$ . We also examine the effect of  $Z_0$  at constant  $X$ . With increased  $Z_0$ , the FBCP evolves towards smaller energies. Eventually, the barrier effects dominate those of  $X$  and the ZBCP resembles that found in the N/S junctions, attributed to midgap surface states [9,11].

In Fig. 4 we illustrate the effect of AA using the parameters from Fig. 3. The solid curves represent AA over all angles below total reflection and the dashed curves are averages over a narrower region. Panel (a) displays the conductance for different polarizations and  $Z_0 = 0$ . The ZBCD reported in [5] resembles the bottommost solid curve. The parameter values for this curve agree with their values in this experiment, as mentioned above. We see that the ZBCD in  $\langle G \rangle$  occurs only at large  $X$ . The curves are then qualitatively different from those found in the tunneling limit for an *s*-wave superconductor, where the peak in  $\langle G \rangle$  is sharp and at the gap energy. In panel (b) we show that formation of ZBCP with increasing  $Z_0$  is a robust feature present in both types of AA.

In Fig. 5 we consider the interplay of FWM and unconventional superconductivity. We take  $L_0 = 1/2$ . In panel (a) we show the results at  $Z_0 = 0$  for a range of values of  $X$ . The ZBCP evolves into a ZBCD. In panel (b) at  $X = 0.7$ , we see that with increasing  $Z_0$  a FBCP forms and then evolves to a ZBCP. The FBCP here has a different origin than the breaking of the time reversal symmetry state in the N/S system [9,11,19]. From Eqs. 1–3 it is simple and instructive to obtain other  $G(E)$  results.

We have shown here that spin polarized tunneling spectroscopy of F/S junctions displays qualitatively novel behavior. The variety of features in  $G(E)$  and  $\langle G(E) \rangle$  arises from the interplay among the form of the pair potential, the exchange energy of a ferromagnet modifying the AR, and the Fermi energies and interface properties of the F and S regions. The results are quite sensitive to FWM

which should be carefully taken into account in interpreting spin polarized experiments and can not, in the polarized case, be simply replaced by a change in parameter  $Z_0$ .

We thank A.M. Goldman, V.A. Vas'ko, K.R. Nikolaev, P.A. Kraus, S.W. Pierson and L. Glazman for discussions.

---

- [1] R.J. Soulen *et al*, Science **282**, 85 (1998).
- [2] S.K. Upadhyay *et al*, Phys. Rev. Lett. **81**, 3247 (1998).
- [3] V.A. Vas'ko *et al*, Phys. Rev. Lett. **78**, 1134 (1997).
- [4] Z.W. Dong *et al*, Appl. Phys. Lett. **71**, 1718 (1997).
- [5] V.A. Vas'ko *et al*, Appl. Phys. Lett. **73**, 844 (1998).
- [6] G. Prinz, Phys. Today **48**, 58 (1995).
- [7] R. Meservey *et al*, Phys. Rep. **238**, 173 (1994).
- [8] M.J.M. de Jong *et al*, Phys. Rev. Lett. **74**, 1657 (1995).
- [9] C.R. Hu, Phys. Rev. Lett **72**, 1526 (1994); J. Yang, and C.R. Hu, Phys. Rev. B **50**, 16 766 (1994).
- [10] J.W. Ekin *et al*, Phys. Rev. B **56**, 13 746 (1997).
- [11] S. Kashiwaya *et al*, Phys. Rev. B **53**, 2667 (1996); Y. Tanaka *et al*, Phys. Rev. Lett. **74**, 3451 (1995).
- [12] A new preprint by J.-X. Zhu *et al* considers some particular cases of F/S junctions without FWM and assuming complete spin polarization independent of  $h_0$ .
- [13] C. Bruder, Phys. Rev. B **41**, 4017 (1990).
- [14] G.E. Blonder *et al*, Phys. Rev. B **25**, 4515 (1982).
- [15] E. Scheer *et al*, Nature **394**, 154 (1998).
- [16] This approximation [13] is valid in our region of interest at subgap conductances. For high bias where its accuracy is reduced,  $G$  is usually dominated by extrinsic effects.
- [17] A.M. Goldman, private communication.
- [18] G.E. Blonder, M. Tinkham, Phys. Rev. B **27**, 112 (1983).
- [19] M. Fogelström *et al*, Phys. Rev. Lett. **79**, 281, (1997).

FIG. 1.  $G(E)$  (Eq. 3).  $E \equiv eV/\Delta_0$ . Results are for  $\theta = 0$  (normal incidence) and  $\alpha = 0$ . The solid curves are for  $L_0 = 1/2$  (FWM present): in panel (a) at  $Z_0 = 0$  (no barrier) they are (from top to bottom at  $E > 1$ ) for exchange energies  $X \equiv h_0/E_F = 0, 0.6, 0.8, 0.968, 0.99, 0.9999$ , while in panel (b) they are at  $X = 0.6$  and (from top to bottom)  $Z_0 = 0, 0.25, 0.5, 1, 1.5$ . The dashed curves are for  $L_0 = 1$  (no FWM). In panel (a)  $X = 0, 0.6, 0.968$ , in panel (b) they are at  $Z_0 = 0, 0.05$ .

FIG. 2.  $\langle G(E) \rangle$ , the  $\theta$  averaged conductivity, for the same parameter values and curve identifications as in Fig. 1. Results in this Figure are averaged over all angles.

FIG. 3.  $G(E)$  for  $\theta = \pi/12$ ,  $\alpha = \pi/4$ , and  $L_0 = 1$ . In (a), at  $Z_0 = 0$ , the curves are for  $X = 0, 0.4, 0.6, 0.7, 0.8, 0.85, 0.9, 0.99$ , (top to bottom at  $E = 0$ .) In (b), the solid curves correspond, from top to bottom at  $E = 2$ , to  $Z_0 = 0, 0.25, 0.5, 1, 1.5$ . The dashed and dash-dotted curves are, respectively, the  $G_\uparrow$  and  $G_\downarrow$  conductances at  $Z_0 = 0$ .

FIG. 4.  $\langle G(E) \rangle$  for the data in Fig. 3. The solid curves are averages over all  $\theta$  while the dashed curves are over a region of width  $\pi/24$  centered at  $\pi/12$ . The curves shown are, respectively, in the same order as those in Fig. 3, except that in (a) results for  $X = 0.4, 0.7, 0.85$  have been excluded for clarity.

FIG. 5.  $G(E)$  for  $\theta = \pi/12$ ,  $\alpha = \pi/4$ , and FWM with  $L_0 = 1/2$ . In (a),  $Z_0 = 0$ , and the curves are for  $X = 0, 0.4, 0.6, 0.7, 0.8, 0.85, 0.9$  (top to bottom at  $E = 0$ ). In (b), the influence of  $Z_0$  is shown for  $X = 0.7$ . The curves correspond, from top to bottom at  $E = 2$ , to  $Z_0 = 0, 0.25, 0.5, 1, 1.5$

Fig 1, Zutic & Valls "Spin polarized.."

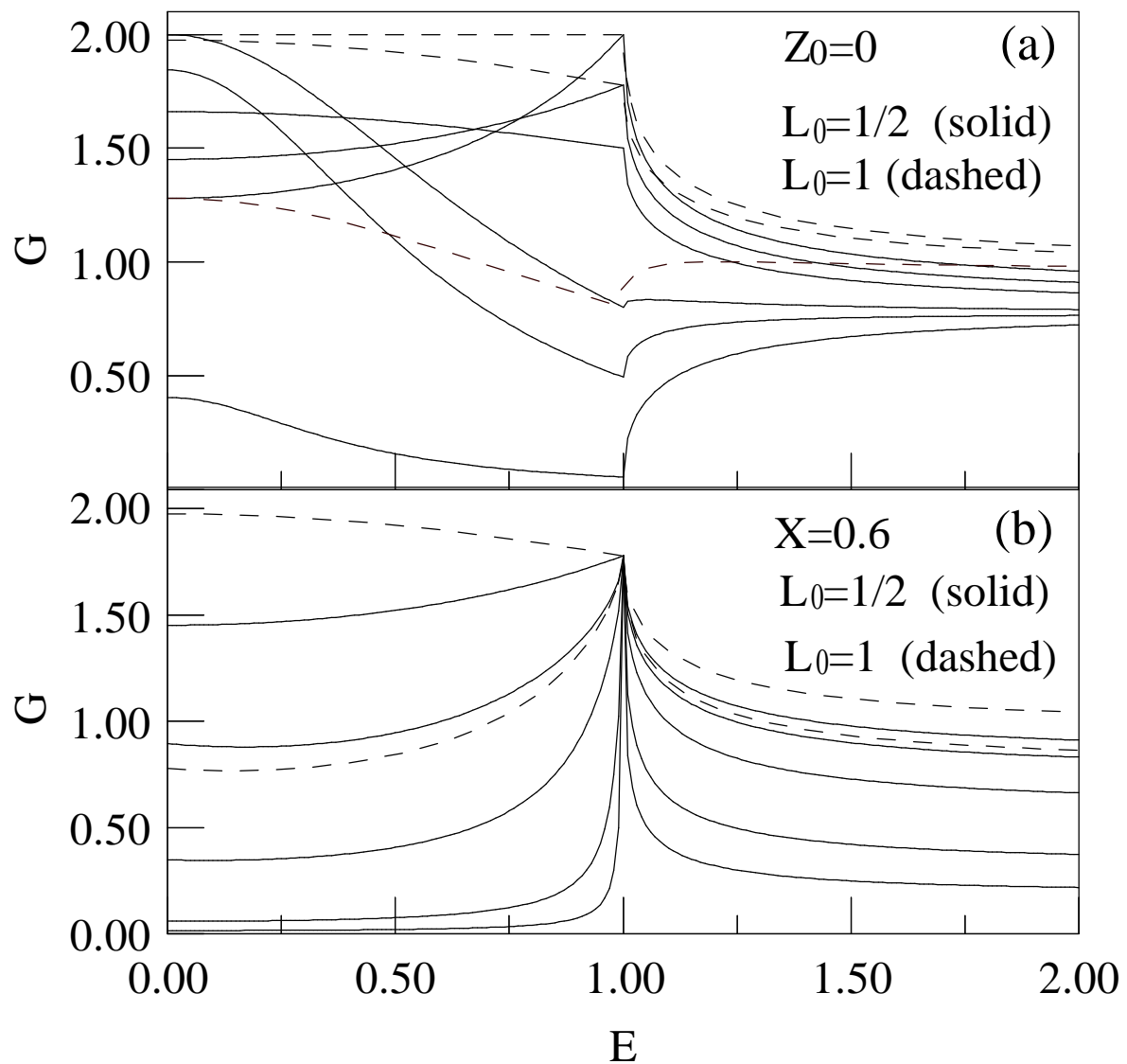


Fig 2, Zutic & Valls "Spin Polarized.."

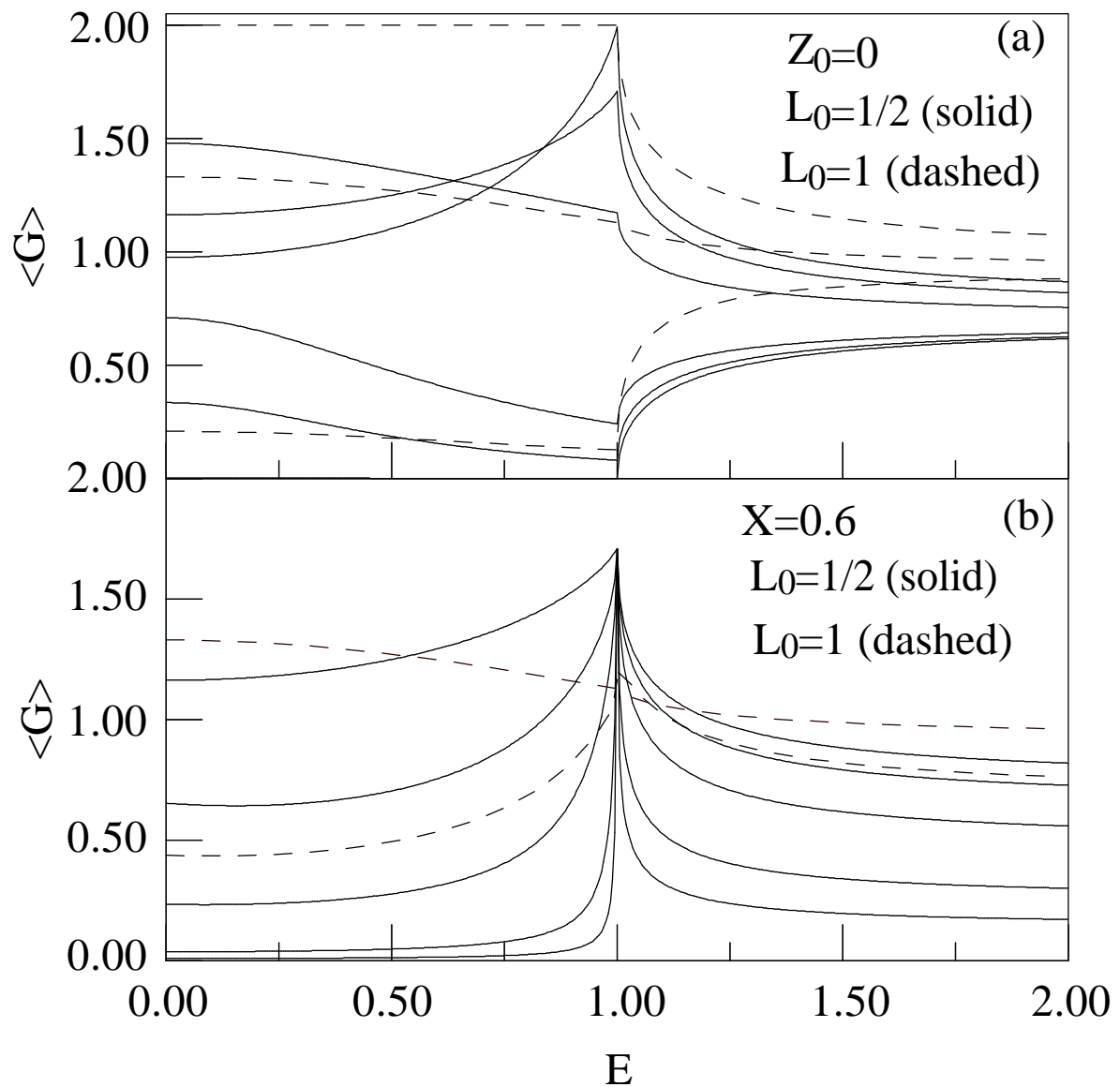


Fig 3, Zutic & Valls "Spin Polarized.."

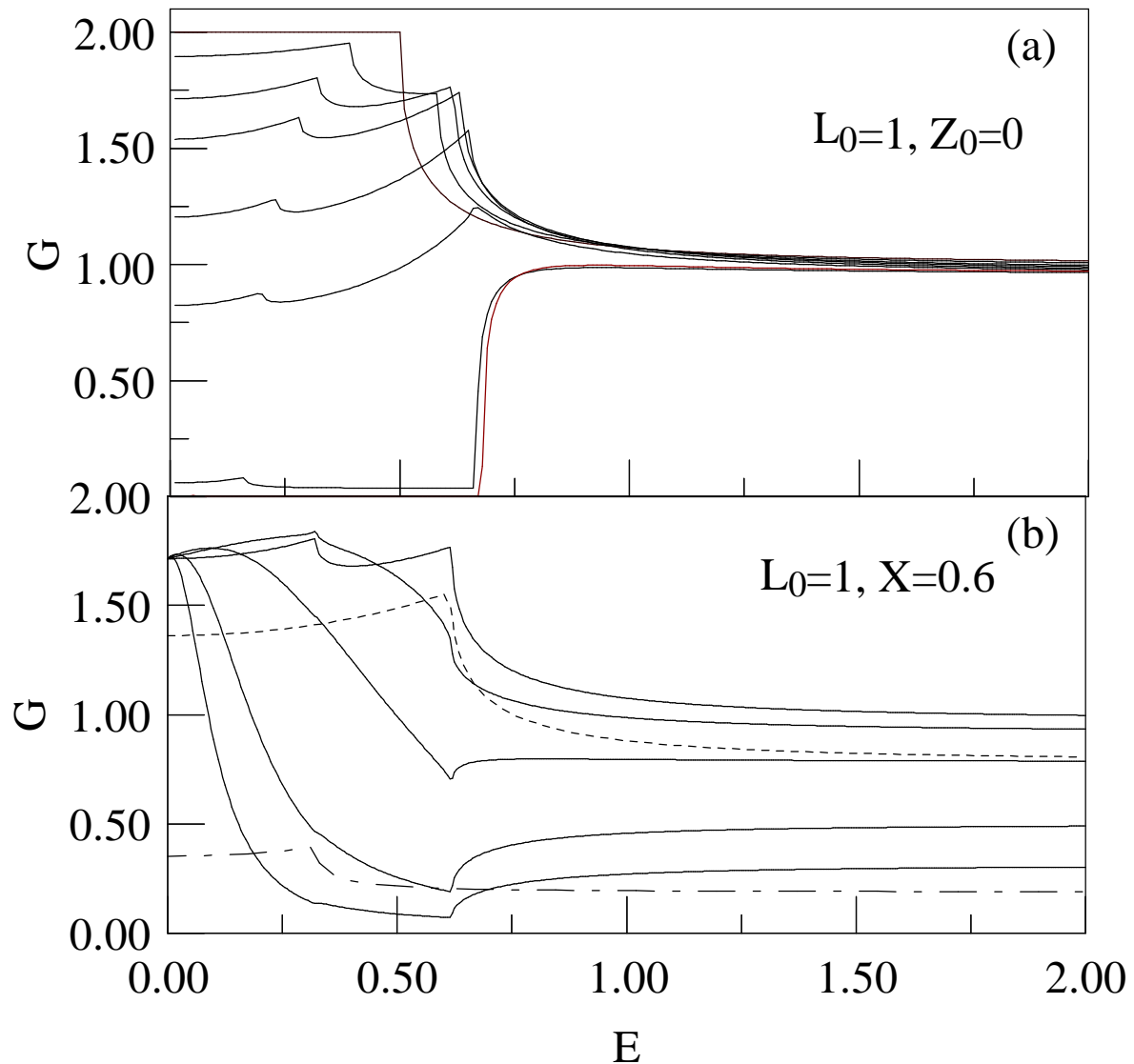


Fig 4, Zutic & Valls "Spin Polarized.."

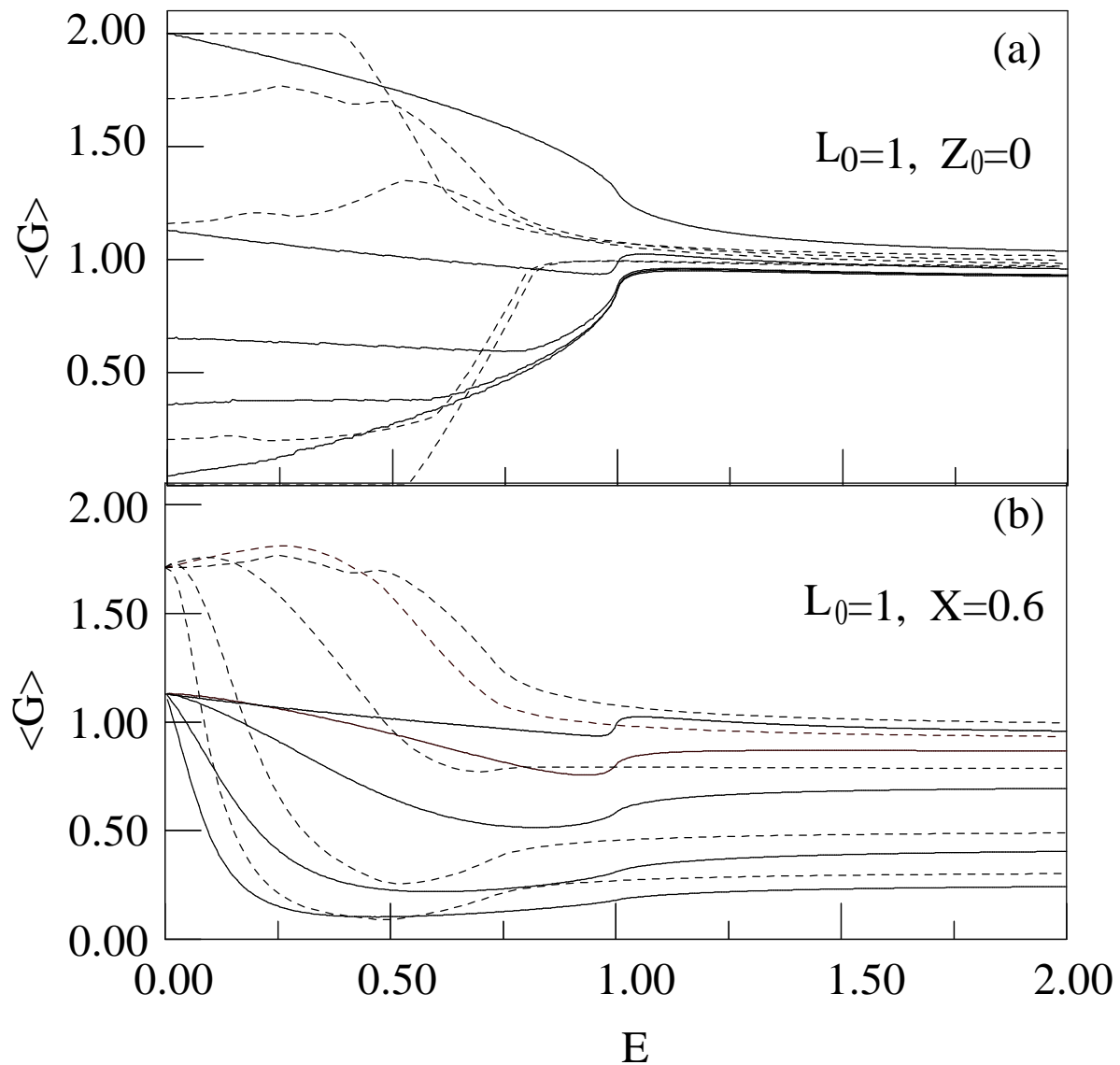


Fig 5, Zutic & Valls "Spin polarized.."

